Journal of Materials Chemistry C

RSC Publishing

PAPER

View Article Online
View Journal | View Issue

Cite this: J. Mater. Chem. C, 2013, 1, 5765

Substitution effects on the electrical tranporting properties of tetrathia[22]annulene[2,1,2,1]: experimental and theoretical investigations†

Jing Zhang,[ad] Zhiying Ma,[b] Qian Zhang,[ad] Tarunpreet Singh Virk,[c] Hua Geng,[a] Dong Wang,[b] Wei Xu,*[a] Zhigang Shuai,*[b] Kamaljit Singh,*[c] Wenping Hu[a] and Daoben Zhu*[a]

Received 25th April 2013
Accepted 14th July 2013

DOI: 10.1039/c3tc30776j

www.rsc.org/MaterialsC

Tetrathia[22]annulene[2,1,2,1] and its derivatives are p-type organic semiconductors possessing relatively high mobilities in thin film field-effect transistors. To get a full understanding of the relationship between the molecular structures and transporting properties of these macrocyclic molecules, the single crystal structures of three *meso*-substituted tetrathia[22]annulene[2,1,2,1]s were determined by X-ray diffraction, and the electrical properties were investigated by single crystal transistor characterization and quantum simulations. The observed relationship between the mobilities of different crystals was strongly corroborated by calculations of both the molecular reorganization energies and the maximum intermolecular transfer integrals.

Introduction

Organic semiconductors (OSCs) have attracted great research interest in the past two decades due to their intrinsic advantages over their inorganic counterparts.[1–8] They are usually solution-processible, facilitating low-cost large-area production, allowing the fabrication of devices, such as photovoltaics, light-emitting diodes and organic integrated circuits on plastic substrates.[9–12] The most important feature of organic semiconductors is that their properties could be easily tuned by the chemical tailoring of the molecular structure.[13–15] In order to get a rational design of organic semiconductors, it is important to explore the structure–property relationships of organic semiconductors, which is currently one of the main areas of research work in OSCs. The organic single crystal field effect transistors (OSCFETs) have been proven to be one of the most powerful tools for probing the relationship between intrinsic electrical transport properties and molecular structures and stacking patterns, as the defects and morphological issues in thin film devices could be minimized.[16–19] Here, OSCFETs based on a series of *meso*-substituted derivatives of tetrathia[22]annulene-[2,1,2,1] (TTA) were fabricated, combined with the device characterization, crystallographic analysis and theoretical analysis, and the structure–property relationship was studied.

Among the organic semiconductors studied to date, π-conjugated molecules with macrocyclic architectures, such as porphyrins and phthalocyanines, have attracted special attention due to their promising optical, electronic, photo-physical properties and self-assembly behavior. High charge carrier mobility has recently been reported for phthalocyanines.[20–23] We found that compared to their linear analogous, macrocyclic conjugated oligomers of triphenylamine, carbazole, pyrrole, or dibenzothiophene exhibited superior transporting properties due to their improved molecular ordering in the solid state and reduced molecular reorganization energies.[24–26] However, due to the nonplanar conformation of these cyclic oligomers, which blocked the more efficient intermolecular electronic coupling, they only possess moderate charge carrier mobilities compared with state-of-the-art materials. For further improvement of the transport properties, TTA, a coplanar aromatic macrocyclic compound was studied recently. The synthesis of tetrathia[22]-annulene[2,1,2,1] (TTA) was first reported by Cava *et al.* nearly two decades ago.[27,28] As a porphyrin like planar aromatic macrocycles with 22 π-electrons, TTA was expected to display improved transport properties compared to that of porphyrins due to the enlarged π-conjugated system which will enhance the intermolecular π–π interactions. However, TTA only displayed moderate mobility (~0.02 $cm^2 V^{-1} s^{-1}$) in thin films, as revealed by thin film OFETs characterization, due to the unfavorable dimerized herringbone stacking pattern.[29] Later, it was

[a]Beijing National Laboratory for Molecular Sciences, Key Laboratory of Organic Solids, Institute of Chemistry, Chinese Academy of Sciences, Beijing, 100190, China. E-mail: wxu@iccas.ac.cn; Tel: +86-10-62423103

[b]Department of Chemistry, Tsinghua University, Beijing, China. E-mail: zgshuai@mail.tsinghua.edu.cn

[c]Organic Synthesis Laboratory, Department of Applied Chemical Sciences & Technology, Guru Nanak Dev University, Amritsar-143005, India. E-mail: kamaljit19in@yahoo.co.in

[d]Graduate School of Chinese Academy of Sciences, Beijing, 100039, China

† Electronic supplementary information (ESI) available. CCDC 936012 and 936013. For ESI and crystallographic data in CIF or other electronic format see DOI: 10.1039/c3tc30776j

found that its transport properties could be significantly improved with phenyl, tolyl or chlorophenyl groups attached at the *meso*-positions (compound **1–3**, Scheme 1).[30] This could be attributed to the molecular stacking pattern change from edge to face (herringbone) packing to face to face (π-stacking) packing which is expected to provide more efficient π-orbital overlap and facilitate charge transport. In order to get a precise relationship between the subtle structure variation effects and the transport properties, we carried out single crystal structure analysis and OSCFETs characterizations, as well as theoretical calculations on compound **1–3**. Such different molecular tailoring motifs of TTA may lead to different transfer integrals and reorganization energies and thus different charge transport properties.[31–35] This investigation will provide guidelines for the further development of organic semiconductors based on such macrocyclic aromatic molecules with improved performance.

Results and discussion

Single crystal structures

The crystallographic data of compound **1** was already reported in an earlier paper,[30] but for comparison it is also presented here. Single crystals of **2** and **3** suitable for X-ray diffraction (XRD) measurements were obtained by evaporating the corresponding solution of **2** or **3** in chloroform, and their crystallographic data is summarized in Table 1. It can be found that slight variation of the peripherally substituted groups leads to obvious changes in both the molecular conformations and their stacking patterns in the crystals. For compound **1** with the phenyl substitutions, the central macrocycle containing four thiophene rings displays an almost coplanar conformation with the sulfur atoms deviating from the mean plane of the central ring by less than 0.1 Å (Fig. 1a). Replacing the phenyl group with a tolyl group makes the planarity of compound **2** decrease a little, as the thiophene rings deviate from the mean plane of the central ring by a dihedral angle of 3–4°, meanwhile, the long axis of peripheral tolyl groups deviates from the central plane with the methyl group carbon atoms (C1) having a distance of 1.6 Å to that plane (Fig. 1c). For compound **3**, the chlorophenyl substitutions make the molecule adopt a highly twisted conformation with the dihedral angles between adjacent thiophene rings in the range of 13.7–22.2° (Fig. 1e). In the crystal, molecule **1** stacks into columns along the *c*-axis, in the column the molecules adopt a slipped face-to-face packing style with the molecules shifted along the short molecular axis and an

Table 1 Crystal data and structure refinement for **2** and **3**

	2	**3**
Formula	$C_{36}H_{26}S_4$	$C_{34}H_{20}Cl_2S_4$
FW	586.81	627.64
Temp. (K)	173(2)	173(2)
Wavelength (Å)	0.71073	0.71073
Crystal system	Triclinic	Triclinic
Space group	$P\bar{1}$	$P\bar{1}$
Unit cell		
a (Å)	7.262(3)	11.102(3)
b (Å)	9.148(5)	11.949(3)
c (Å)	11.131(5)	12.195(3)
α (°)	102.635(8)	108.950(2)
β (°)	94.961(7)	112.420(2)
γ (°)	106.756(5)	95.820(2)
Volume (Å^3)	682.1(6)	1366.7(5)
Z	1	2
Abs. co. (mm^{-1})	0.375	0.569
F (000)	306	644
Crys. size (mm)	0.22 × 0.11 × 0.03	0.15 × 0.12 × 0.05
θ range (°)	2.40 to 27.47	1.86 to 27.49
Limiting indices	$-9 \le h \le 9$	$-14 \le h \le 14$
	$-11 \le k \le 11$	$-15 \le k \le 15$
	$-14 \le l \le 10$	$-15 \le l \le 15$
Reflec. collected	6509	15 405
Unique	3105	6247
R(int)	0.0457	0.0447
Abs. correction	Semi-empirical from equivalents	
Refin. method	Full-matrix least-squares on F^2	
Data/restr./para.	3105/0/182	6247/0/361
S	1.080	1.117
R [$I > 2$sigma(I)]	$R1 = 0.0462$	$R1 = 0.0455$
	w$R2 = 0.1180$	w$R2 = 0.1041$
R (all data)	$R1 = 0.0496$	$R1 = 0.0525$
	w$R2 = 0.1213$	w$R2 = 0.1078$

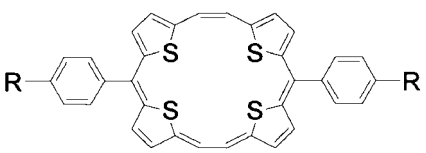

1: R = H

2: R = CH$_3$

3: R = Cl

Scheme 1 Chemical structure of compounds **1**, **2**, and **3** (*meso*-substituted tetrathia[22]annulene[2,1,2,1]) and their different terminal groups.

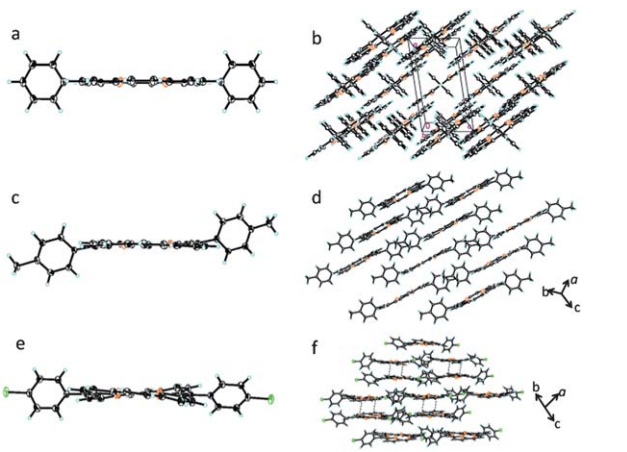

Fig. 1 Crystal structures of **1–3**. Side view of the molecular structure of **1** (a), **2** (c) and **3** (e) with 50% probability ellipsoids in the crystals. Stacking pattern of **1** (b), **2** (d) and **3** (f) in the crystals.

interplanar distance of 3.53 Å (Fig. 1b). As shown in Fig. 1d, compound **2** packs in a similar slipped face-to-face pattern in the crystals, but the molecule is shifted along the long molecular axis with an interplanar distance of 3.66 Å (Fig. 1d). But for compound **3** with a Cl tail, the molecules form dimers through intermolecular S···S interactions, and these dimers further pack into shifted face-to-face patterns along the *c*-axis. It can be seen that all these compounds show shifted face-to-face packing in the crystals, which is different from that of the dimerized herringbone pattern of tetrathia[22]annulene[2,1,2,1]. So, the attaching of these substitution groups not only leads to an increase in the solubility and slightly different redox behaviors, but also leads to dramatic changes in molecular packing in the solid state. Variations of the solid-state properties, such as the charge-carrier mobility, can also be expected. This series of annulene derivatives will allow us to derive relationships between molecular packing structures and the performance of materials.

The molecular structures of compounds **1–3** have been optimized and their frontier molecular orbitals, as well as reorganization energies, have been obtained at the B3LYP/6-31G(d) level with the Gaussian 09 package.[36] Two isomers, *i.e.* the parallel form and staggered form, have been identified for each compound, which differ in the relative orientation of the two substitution groups in the *para*-position (see Fig. S1 in the ESI†). Because of the steric hindrance of the substitutions, the central macrocycle for the parallel form maintains the planarity, while for the staggered form, it is twisted. Moreover, the staggered conformer is only stabilized by about 10 meV relative to the parallel one. It appears that compounds **1** and **2** adopt the parallel conformation in the crystal, while compound **3** adopts the staggered conformation. Since both conformers are stable, which conformation is adopted in the crystal depends on the crystallization conditions and intermolecular interactions.

The charge densities of the HOMO and LUMO presented in Fig. 2 are mainly delocalized on the cyclic conjugated backbone, and minor charge density distribution was found on substitution groups. Therefore, substitutions have little effect on frontier molecular orbitals. To see the stability of these three systems, both the adiabatic ionization energies (AIE) and vertical ionization energies (VIE) were calculated. As provided in Table 2, the AIE and VIE values fall into the range of IE values for air-stable p-channel materials (from 5.68 eV to 6.78 eV) discovered in previous studies.[37]

Intramolecular vibronic coupling, *i.e.* the reorganization energy has been calculated based on normal-mode analysis.[38] As presented in Table 2, the reorganization energy of system **1** is very close to that of system **2**, both adopting the parallel conformation, while system **3** in the staggered conformation shows a little smaller reorganization energy. The reorganization energies of compounds **1–3** in both conformations have been calculated, and it is revealed that the reorganization energy is influenced mainly by the molecular conformation, not the chemical substitution. The reorganization energy for the parallel conformer is a few tens of meV larger than that for the corresponding staggered conformer, but overall the difference is not significant. As will be shown below, chemical substitution here affects the transport properties mainly by affecting the molecular packing and transfer integrals. Partition of the intramolecular relaxation energy into contributions from different vibrational modes (see Fig. S2†) reveals that contributions from the vibrational modes of both the neutral and cationic state of the system **1** are quite similar to those of system **2**, with both adopting a parallel conformation in the crystal. For system **3** adopting the staggered conformation, the low frequency vibrational modes with major contributions to the reorganization energy undergo some changes, in both the neutral and cationic states, compared to those for systems **1** and **2**. This is because the structural relaxation between the cationic state and the neutral state is small in the staggered conformation, thus, the contribution to the reorganization energy from the low frequency vibrations for system **3** decreases compared to those for systems **1** and **2**. Moreover, from Fig. S2† we found not only a low frequency vibration due to the twisting of terminal groups (below 100 cm^{-1}), but also a high frequency C=C in-plane stretching vibration in the central macrocycle (around 1500 cm^{-1}) play an important role in charge-transfer relaxation processes for all three systems. While scatterings with low-frequency vibration could be approximated by Marcus semiclassical treatment, the high-frequency vibration should be treated fully quantum mechanically taking all the vibrational modes into account, and the high-frequency vibration has been shown to exhibit a quantum nuclear tunnelling effect.[39] Such an effect has been confirmed experimentally.[40]

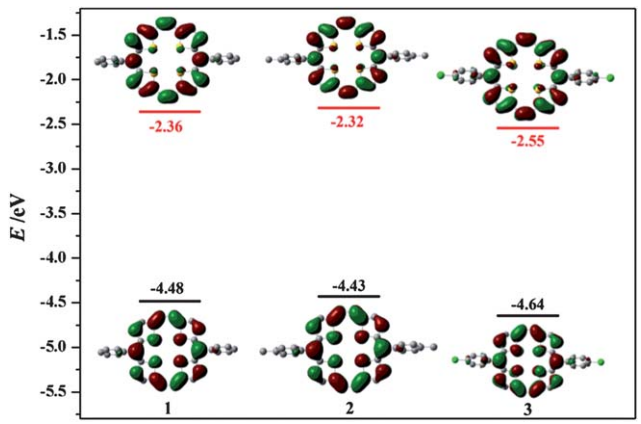

Fig. 2 Illustration of the frontier molecular orbitals for **1–3**.

Table 2 Computed adiabatic ionization energy (AIE) and vertical ionization energy (VIE) (in eV) and the reorganization energies (in meV). NM (normal mode) represents the summation over all the displaced harmonic oscillators

	AIE[a]	VIE[a]	NM[b]
1	5.74	5.82	232 (187)
2	5.66	5.75	238 (217)
3	5.86	5.94	196 (243)

[a] A single-point energy calculation was performed to calculate the ionization energy at the B3LYP/6-31+G* level based on the optimized geometries at the B3LYP/6-31G* level. [b] The values in the parentheses refer to the reorganization energy for the conformation not showing in the crystal structure, as mentioned in Fig. S1.

Single crystal field-effect transistors

Fig. 3a, c and e show the scanning electron microscopy (SEM) images of **1–3** self-assembled single crystals from chlorobenzene (1 mg mL^{-1}) at room temperature using a drop-casting method in ambient conditions. Compound **1** formed flexible 1D micro/nanometer wires with diameters from hundreds of nanometers to several micrometers and lengths of hundreds to thousands of micrometers (Fig. 3a), compound **2** formed 2D microribbons with widths of several to tens of micrometers and lengths from tens to hundreds of micrometers (Fig. 3c), and compound **3** displays microplates with widths of several to tens of micrometers and lengths from several to tens of micrometers (Fig. 3e). The power X-ray diffraction patterns of theses wires/ribbons/plates show intense peaks corresponding to the crystallographic data of the molecules **1–3** (Fig. 3b, d and f). It is well-known that the assembly morphologies are controlled by their intermolecular interactions. Such 1D micro/nanometer wire to microplate morphology transformation of these derivative materials indicated the remarkable changes of the intermolecular interactions of compounds **1–3** as a result of the different substitute groups, which could be proven by their single crystal diffraction results as follows.

The charge transport properties of **1–3** were examined to study their potential applications in OFETs. First, the above single crystal micro/nanometer wires, ribbons or plates were grown directly on *n*-octadecyltrichlorosilane (OTS) treated SiO_2/Si substrates *via* drop-casting from chlorobenzene solutions. Then transistors were fabricated *in situ* by evaporating Au films (~50 nm) onto these micro/nanometer wires, ribbons or plates as source–drain electrodes. Fig. 4a shows the schematic structure of a single crystalline FET (SCFET) fabricated through such a method. Fig. 4b–d show the corresponding optical images of the SCFET devices. All the SCFETs exhibited typical p-type properties under ambient conditions. Typical transfer and output characteristics of the SCFETs are shown in Fig. 5. The best results are obtained from devices of **1**, which shows the highest mobility of 0.7 $cm^2 V^{-1} s^{-1}$ with an average mobility of 0.4 $cm^2 V^{-1} s^{-1}$. Here, the mobilities (μ) were calculated in the saturation regime by the following eqn (1):

$$I_D = \mu C_i (W/2L)(V_G - V_D)^2 \quad (1)$$

where I_D is the drain current, μ is the field-effect mobility, C_i is the gate dielectric capacitance, W and L are the channel width and length, respectively, and V_T is the threshold voltage. Based on the individual single-crystalline ribbons of **1–3**, more than 60 SCFET devices were fabricated and examined. The mobilities were in the range of 0.08 to 0.7 $cm^2 V^{-1} s^{-1}$ for **1**, 0.03 to 0.4 $cm^2 V^{-1} s^{-1}$ for **2** and 0.005 to 0.2 $cm^2 V^{-1} s^{-1}$ for **3**, respectively. It is noticed that the mobilities of the devices exhibit a relatively wide distribution, which might be due to the difference in the quality of the crystals and the influence of contact conditions at the semiconductor–dielectric and semiconductor–electrode interfaces. It is well known that many factors, such as the position and deposition process of the source–drain electrodes, *i.e.*, the precise orientation of the electrodes with respect to the π-stacking axis of the crystals, the gate electrode, the used material and flatness of the insulating layer, the quality of the crystal and crystal–insulator interface, *etc.* could affect the device performance, *i.e.*, the value of the mobility. Micro/nanowires of compound **1** could get as long as milimetres and it was found that nearly 90% of the devices of compound **1** exhibited a mobility >0.1 $cm^2 V^{-1} s^{-1}$ with a highest mobility of 0.7 $cm^2 V^{-1} s^{-1}$, which indicates the prospective future of these compounds in organic electronics.

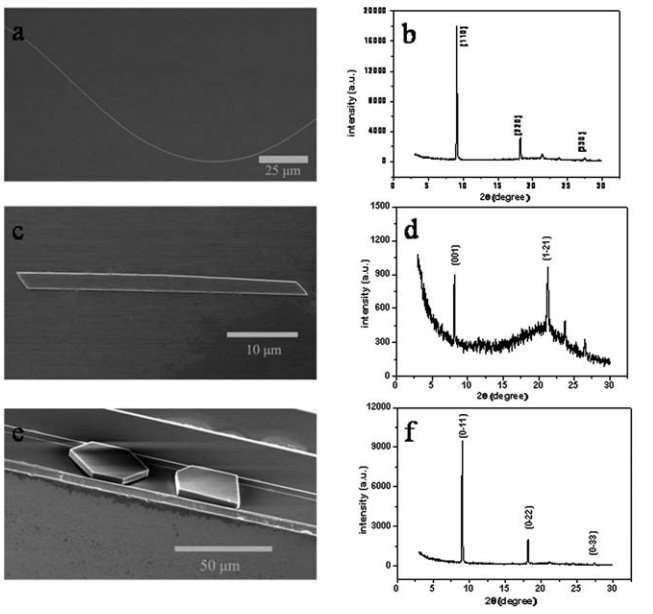

Fig. 3 (a, c and e) SEM images of an individual wire, ribbon and plates of **1**, **2** and **3** single crystals produced by the drop-casting method. (b, d and f) Power diffraction patterns of the wires, ribbons and plates, the peaks were indexed with lattice constants of the bulk crystals.

Charge transport pathways

Based on the crystal structures of systems **1–3** and the calculated transfer integrals, the main charge transfer pathways were discovered and illustrated in Fig. 6. Here, the site energy correction method[41] was adopted to calculate transfer integrals at the PW91PW91/6-31G* level. As presented in the Fig. 6, system **1** displays one-dimensional transport character along the *c*-axis (*i.e.* along P3 and P4). The intermolecular distance along other pathways is so large that the transfer integral is very small. Compared to system **1**, two tolyl group substitutions induce a very different crystal structure of system **2**. The system displays two-dimensional transport behavior, but the transfer integrals along all the pathways are smaller than those of P3 and P4 in the system **1**. A two-dimensional transport network has also been found for system **3**. However, the molecule with chlorophenyl substitutions adopts a highly twisted conformation, which does not favor π–π stacking, and the electronic couplings of the P3 and P4 pathways decreased to 1.80 and 9.36 meV respectively. These results can be rationalized by an analysis of the relative positions of the interacting molecules and the shape of the HOMO of a single molecule. The transfer integral increases if both overlapping orbitals are either

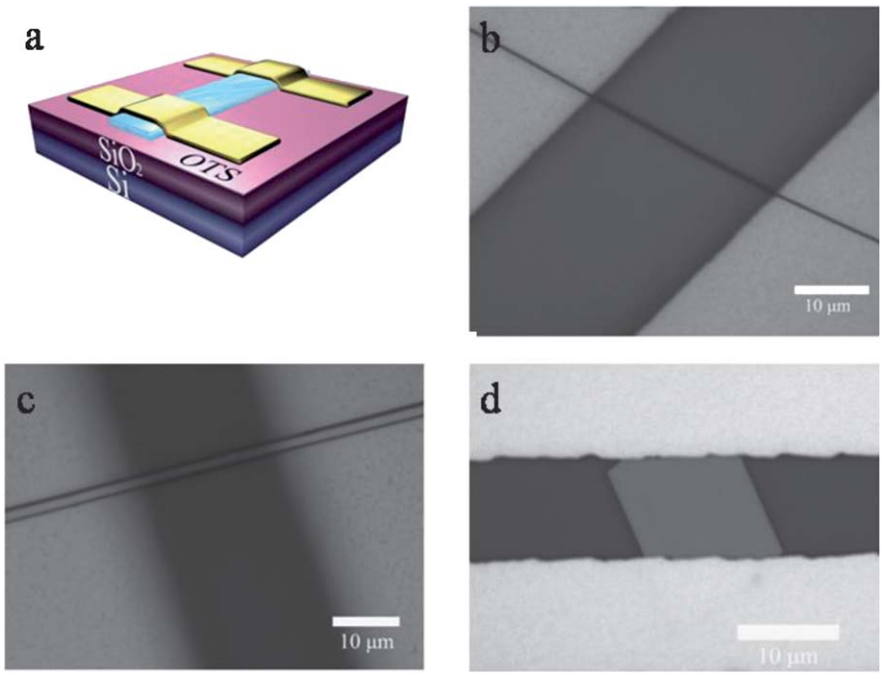

Fig. 4 (a) The schematic structure of a SCFET fabricated by such a method. (b, c and d) The optical images of an example device based on an individual single crystal of **1**, **2** and **3**.

bonding or antibonding, while it decreases if there exists a cancellation between the bonding and antibonding overlap.[42] The relative positions of the dimers and the molecular orbitals along the pathways displaying the maximal transfer integrals are highlighted in Fig. S3.† It can be seen that the displacement in system **3** along the short molecular axis is smaller than that in system **1** (see Fig. S3(b)†). Moreover, there exists minor displacement along the long molecular axis in the system **3**. Both displacements will result in a cancellation of bonding and antibonding overlap (see Fig. S3(c) and (e)†). Thus, the transfer integral along P2 in system **3** is smaller than that along P3 in system **1**. For system **2**, the molecule slips along the long molecular axis. The relative position of the dimer and the shape of the HOMO do not favor orbital overlap, as can be seen from Fig. S3(d) and (e),† thus the corresponding transfer intergral is smaller than that of P3 in system **1** as shown in Fig. 6.

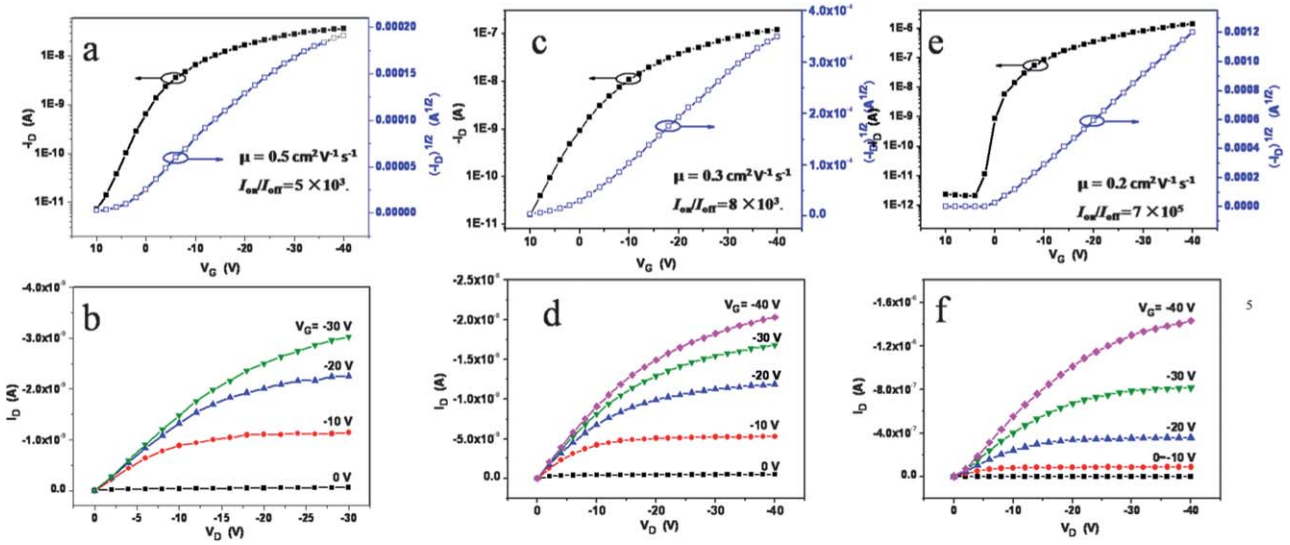

Fig. 5 (a) Typical transfer curve ($V_D = -40$ V) and (b) the corresponding output curve of a SCFET based on an individual single-crystalline wire of **1**, with W/L = 0.17 μm/11.3 μm. (c) Typical transfer curve ($V_D = -60$ V) and (d) the corresponding output curve of a SCFET based on an individual single-crystalline ribbon of **2**, with W/L = 2.1 μm/28.8 μm. (e) Typical transfer curve ($V_D = -40$ V) and (f) the corresponding output curve of a SCFET based on an individual single-crystalline ribbon of **3**, with W/L = 13.0 μm/10.3 μm.

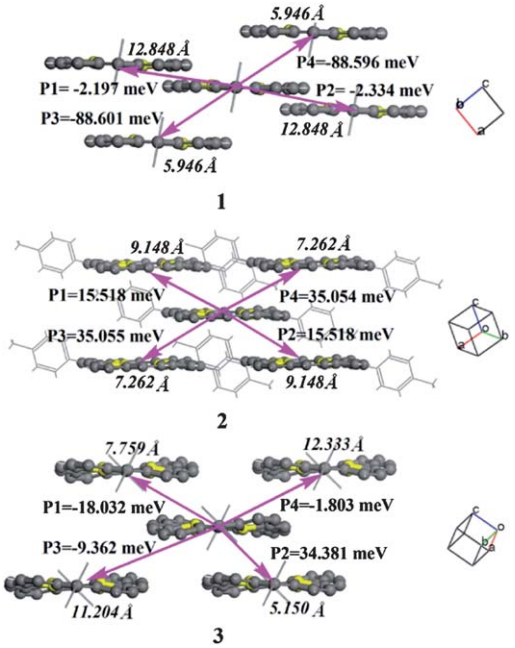

Fig. 6 The main transport networks, the distances of the centroid (in italics) and transfer integrals between the two molecules.

Based on the above analysis of the charge transfer parameters, we found that the reorganization energy is much larger than the electronic coupling for this series of materials. Therefore, the tunnelling enabled the adoption of a hopping model to estimate the charge carrier mobility of these three systems.[39] System **1** exhibits the largest charge mobility up to 10.64 $cm^2\ V^{-1}\ s^{-1}$ along the *c*-axis, which is one order-of-magnitude higher than the experimental value. However, we know that one-dimensional charge transport is more susceptible to dopant and experimental conditions. In contrast, two-dimensional diffusions have been found for both system **2** and system **3**, and their charge mobilities are 1.18 $cm^2\ V^{-1}\ s^{-1}$ and 0.45 $cm^2\ V^{-1}\ s^{-1}$, respectively, which are in better agreement with the experimental values. In the sense of structure–property relationships, the charge mobilities of the three substituents based on theoretical prediction are in qualitative agreement with the experimental results.

Experimental

With slow evaporation of about 1 mg mL^{-1} chlorobenzene solution, we obtained microscopic crystalline objects of compounds **1–3** through the simple drop-casting method. Scanning electron microscopy (SEM) images were obtained with a Hitachi S-4300SE scanning electron microscope. Optical images were captured with a Leica DM 400M microscope. The structures were analyzed by powder XRD (Rigaku D/max 2500). Transistor characteristics were recorded with a Keithley 4200 SCS and a Micromanipulator 6150 probe station in a clean and shielded box at room temperature.

Conclusions

In this paper, we obtained and fully investigated three *meso*-substituted derivatives of tetrathia[22]annulene[2,1,2,1]. The effect of chemical substitutions on the molecular packing and electronic properties of the organic semiconductors were examined. The introduction of tail groups was proven not only to enhance the solubility and self-organization of the compounds, but also shifted the molecular packing from herringbone to face-to-face π–π stacking. The subtle changes of molecular structure brought remarkable changes in the molecular packing, crystallinity, and thus device performance, indicating the importance of chemical substitutions as a powerful molecular design tool to tune the packing motifs of organic semiconductors and their corresponding electronic properties. We also calculated the transport properties of holes. The structural, electronic, and transport properties were calculated in terms of the molecular frontier orbitals, ionization potentials, and reorganization energies of the monomers and the electronic coupling between adjacent molecules.

Acknowledgements

This work was supported by the National Natural Science Foundation of China (21290191, 20952001, 21021091), the National Major State Basic Research Development Program (2011CB808401, 2011CB932304), and the Chinese Academy of Sciences. KS thanks DST, New Delhi for financial assistance (Project: SR/S1/OC-27/2009).

References

1 G. Horowitz, *Adv. Mater.*, 1998, **10**, 365–377.
2 T. P. I. Saragi, T. Spehr, A. Siebert, T. Fuhrmann-Lieker and J. Salbeck, *Chem. Rev.*, 2007, **107**, 1011–1065.
3 J. Zaumseil and H. Sirringhaus, *Chem. Rev.*, 2007, **107**, 1296.
4 H. Klauk, *Chem. Soc. Rev.*, 2010, **39**, 2643.
5 M. Mas-Torrent and C. Rovira, *Chem. Soc. Rev.*, 2008, **37**, 827.
6 Y. Sun, Y. Liu and D. Zhu, *J. Mater. Chem.*, 2005, **15**, 53.
7 M. E. Roberts, A. N. Sokolov and Z. Bao, *J. Mater. Chem.*, 2009, **19**, 3351.
8 P. Lin and F. Yan, *Adv. Mater.*, 2012, **24**, 34.
9 G. H. Gelinck, H. E. A. Huitema, E. Van Veenendaal, E. Cantatore, L. Schrijnemakers, J. Van der Putten, T. C. T. Geuns, M. Beenhakkers, J. B. Giesbers, B. H. Huisman, E. J. Meijer, E. M. Benito, F. J. Touwslager, A. W. Marsman, B. J. E. Van Rens and D. M. De Leeuw, *Nat. Mater.*, 2004, **3**, 106.
10 Y. Zhao, C.-a. Di, X. Gao, Y. Hu, Y. Guo, L. Zhang, Y. Liu, J. Wang, W. Hu and D. Zhu, *Adv. Mater.*, 2011, **23**, 2448.
11 H. Klauk, U. Zschieschang, J. Pflaum and M. Halik, *Nature*, 2007, **445**, 745.
12 T. Sekitani, U. Zschieschang, H. Klauk and T. Someya, *Nat. Mater.*, 2010, **9**, 1015.
13 G. Zhao, H. Dong, H. Zhao, L. Jiang, X. Zhang, J. Tan, Q. Meng and W. Hu, *J. Mater. Chem.*, 2012, **22**, 4409.

14 C. Wang, H. Dong, W. Hu, Y. Liu and D. Zhu, *Chem. Rev.*, 2012, **112**, 2208.
15 M. L. Tang, A. D. Reichardt, P. Wei and Z. Bao, *J. Am. Chem. Soc.*, 2009, **131**, 5264.
16 J. E. Anthony, *Chem. Rev.*, 2006, **106**, 5028.
17 F. Würthner and R. Schmidt, *ChemPhysChem*, 2006, **7**, 793.
18 Z. Wei, W. Hong, H. Geng, C. Wang, Y. Liu, R. Li, W. Xu, Z. Shuai, W. Hu, Q. Wang and D. Zhu, *Adv. Mater.*, 2010, **22**, 2458.
19 Z. Bao, A. J. Lovinger and A. Dodabalapur, *Appl. Phys. Lett.*, 1996, **69**, 3066.
20 Q. Tang, L. Jiang, Y. Tong, H. Li, Y. Liu, Z. Wang, W. Hu, Y. Liu and D. Zhu, *Adv. Mater.*, 2008, **20**, 2947.
21 Q. Tang, Y. Tong, W. Hu, Q. Wan and T. Bjørnholm, *Adv. Mater.*, 2009, **21**, 4234.
22 Z. Wei, W. Xu, W. Hu and D. Zhu, *Langmuir*, 2009, **25**, 3349.
23 Y. Song, C. a. Di, X. Yang, S. Li, W. Xu, Y. Liu, L. Yang, Z. Shuai, D. Zhang and D. Zhu, *J. Am. Chem. Soc.*, 2006, **128**, 15940.
24 Y. Song, C.-a. Di, Z. Wei, T. Zhao, W. Xu, Y. Liu, D. Zhang and D. Zhu, *Chem.–Eur. J.*, 2008, **14**, 4731.
25 Y. B. Song, C. A. Di, W. Xu, Y. Q. Liu, D. Q. Zhang and D. B. Zhu, *J. Mater. Chem.*, 2007, **17**, 4483.
26 H. Xu, G. Yu, W. Xu, Y. Xu, G. Cui, D. Zhang, Y. Liu and D. Zhu, *Langmuir*, 2005, **21**, 5391.
27 Z. Hu, J. L. Atwood and M. P. Cava, *J. Org. Chem.*, 1994, **59**, 8071.
28 Z. Hu and M. P. Cava, *Tetrahedron Lett.*, 1994, **35**, 3493.
29 T. Zhao, Z. Wei, Y. Song, W. Xu, W. Hu and D. Zhu, *J. Mater. Chem.*, 2007, **17**, 4377.
30 K. Singh, A. Sharma, J. Zhang, W. Xu and D. Zhu, *Chem. Commun.*, 2011, **47**, 905.
31 M. Malagoli and J. L. Brédas, *Chem. Phys. Lett.*, 2000, **327**, 13.
32 J. L. Brédas, J. P. Calbert, D. A. da Silva and J. Cornil, *Proc. Natl. Acad. Sci. U. S. A.*, 2002, **99**, 5804.
33 V. Coropceanu, J. Cornil, D. A. da Silva Filho, Y. Olivier, R. Silbey and J.-L. Brédas, *Chem. Rev.*, 2007, **107**, 926.
34 L. Wang, G. Nan, X. Yang, Q. Peng, Q. Li and Z. Shuai, *Chem. Soc. Rev.*, 2010, **39**, 423.
35 Z. Shuai, L. Wang and Q. Li, *Adv. Mater.*, 2011, **23**, 1145.
36 M. J. Frisch, G. W. Trucks, H. B. Schlegel, G. E. Scuseria, M. A. Robb, J. R. Cheeseman, G. Scalmani, V. Barone, B. Mennucci, G. A. Petersson, H. Nakatsuji, M. Caricato, X. Li, H. P. Hratchian, A. F. Izmaylov, J. Bloino, G. Zheng, J. L. Sonnenberg, M. Hada, M. Ehara, K. Toyota, R. Fukuda, J. Hasegawa, M. Ishida, T. Nakajima, Y. Honda, O. Kitao, H. Nakai, T. Vreven, J. A. Montgomery, Jr, J. E. Peralta, F. Ogliaro, M. Bearpark, J. J. Heyd, E. Brothers, K. N. Kudin, V. N. Staroverov, R. Kobayashi, J. Normand, K. Raghavachari, A. Rendell, J. C. Burant, S. S. Iyengar, J. Tomasi, M. Cossi, N. Rega, J. M. Millam, M. Klene, J. E. Knox, J. B. Cross, V. Bakken, C. Adamo, J. Jaramillo, R. Gomperts, R. E. Stratmann, O. Yazyev, A. J. Austin, R. Cammi, C. Pomelli, J. W. Ochterski, R. L. Martin, K. Morokuma, V. G. Zakrzewski, G. A. Voth, P. Salvador, J. J. Dannenberg, S. Dapprich, A. D. Daniels, O. Farkas, J. B. Foresman, J. V. Ortiz, J. Cioslowski and D. J. Fox, *Gaussian 09, Revision A.02*, Gaussian, Inc., Wallingford CT, 2009.
37 C. Liu, S. W. Mao and M. Kuo, *J. Phys. Chem. C*, 2010, **114**, 22316.
38 J. Reimers, *J. Chem. Phys.*, 2001, **115**, 9103.
39 H. Geng, Q. Peng, L. Wang, H. Li, Y. Liao, Z. Ma and Z. Shuai, *Adv. Mater.*, 2012, **24**, 3568.
40 K. Asadi, *et al.*, *Nat. Commun.*, 2013, **4**, 1710, DOI: 10.1038/ncomms2708.
41 E. Valeev, V. Coropceanu, D. da Silva Filho, S. Salman and J. Brédas, *J. Am. Chem. Soc.*, 2006, **128**, 9882.
42 X. Yang, L. Wang, C. Wang, W. Long and Z. Shuai, *Chem. Mater.*, 2008, **20**, 3205.